330 MHz VLA OBSERVATIONS OF 20 GALACTIC SUPERNOVA REMNANTS

NAMIR E. KASSIM
Code 4215.3, Center for Advanced Space Sensing, Naval Research Laboratory, Washington, DC 20375-5000
Received 13 August 1991; revised 19 November 1991

ABSTRACT

We present 330 MHz images and integrated flux densities for 20 previously identified 1st quadrant Galactic Supernova Remnants (SNRs). The observations were made in the D configuration of the VLA giving an angular resolution of $\sim 3'$ and providing good sensitivity to extended structure. Such emission, particularly if it is nonthermal, might be missed on higher frequency surveys due to confusion with the Galactic background and confusion with thermal sources in complex regions. Both problems are reduced by interferometric observations at this lower frequency. The flux densities presented can be used to anchor the low frequency end of the radio spectra of these sources, which are often poorly determined by previous observations at both high and low frequencies. The measurements presented here are also useful for distinguishing steeper spectrum shell-type emission from flatter spectrum plerionic emission for SNRs whose intrinsic morphological type is not well established.

1. INTRODUCTION

A major obstacle to numerous problems in Galactic astrophysics arises from the well known incompleteness of existing Galactic Supernova Remnant (SNR) catalogs (Green 1984, 1988a, 1991). One reason for this is the selection effect imposed by the surface-brightness sensitivity and dynamic range limitation of centimeter wavelength radio continuum surveys in the Galactic plane, selecting against SNRs or parts of SNRs with low level diffuse emission (Green 1988b).

For the same reason, the properties of identified Galactic SNRs are often poorly known, in particular their radio spectral index and total extent. In deriving continuum spectra for 36 1st quadrant Galactic SNRs, Kassim (1989a,b) often found widely conflicting flux density measurements for the same objects at similar frequencies. The confusion is enhanced for directions toward the inner Galaxy where the Galactic background emission is high and insufficient angular resolution imposes confusion with thermal sources in complex regions.

In order to address these difficulties, we have undertaken a program to study Galactic SNRs using the VLA[1] at 330 MHz (P band). In its D configuration (providing maximum surface-brightness sensitivity), the VLA P-band system is ideal for this purpose. First, the contrast between thermal and nonthermal emission is often greater at P band than at higher frequencies, thus allowing easier separation of thermal and nonthermal sources in complex regions (e.g., see Kassim & Weiler 1990a,b). Second, in its D configuration the VLA at 330 MHz is sensitive to low surface-brightness emission from extended ($\leqslant 45'$) SNRs, but is not confused with the much more extended ($> 2°$) Galactic background resolved out by the interferometer. Furthermore, Kassim (1989b) has shown that 330 MHz is a sufficiently high frequency so that absorption of nonthermal emission by all but discrete, high density H II regions lying along the line of sight is negligible.

Flux densities provided by such measurements are therefore useful for anchoring the low frequency end of the intrinsic spectra of these nonthermal sources. For example, Kassim *et al.* (1991) observed the CTB37A/B SNR complex with the same VLA P-band system. Their observations revealed large areas of extended, low surface-brightness emission associated with known SNRs in the complex that were missed by previous observations, and also led to the identification of a new Galactic SNR.

In this paper, we present 330 MHz maps and integrated flux densities for 20 previously identified Galactic SNRs. In addition to providing improved information on their continuum spectra and angular extent, these new low frequency measurements should aid in the classification of the SNR morphological type. Specifically, low frequency measurements can help distinguish between flatter spectrum plerionic and steeper spectrum shell-type emission [e.g., see Weiler & Sramek (1988) for a discussion of the differences between plerions and shell-type SNRs]. Some of the maps may also be useful for separation of thermal and nonthermal emission from SNRs superimposed on thermal sources in complex regions (e.g., W51, Odegard & Kassim 1992). Results from our observations pertaining to known H II regions, SNR candidates, and previously unidentified sources will be presented separately. The observations presented here are not ideal for studying fine structure in the brightness distributions; these details can be better studied with observations using the improved and much more sensitive P-band system currently on-line at the VLA, and by observations in larger array configurations which employ full three-dimensional imaging algorithms.

2. OBSERVATIONS

Observations toward 20 SNRs in the first Galactic quadrant were obtained with the VLA P-band (90 cm, 327–333 MHz) system during two separate runs in the D configuration (maximum baseline ~ 1 km) on 20 March 1987 (15 P-band antennas available) and 8 July 1988 (22 P-band antennas available). In both cases, observations were made in two 3 MHz bands centered at 327.5 MHz and 333.0 MHz (λ 90 cm). For each phase center, the total integration time was approximately 1 hr, consisting of six 10^m snapshots spread over an 8 hr time period in order to optimize the available uv coverage. Table 1 summarizes the number of P-band antennas and uv ranges obtained for each SNR observed.

[1] The VLA is a facility of the National Radio Astronomy Observatory operated by Associated Universities, Inc., under a cooperative agreement with the National Science Foundation.

TABLE 1. Observed parameters for 20 Galactic SNRs.

Name	R.A. (1950.0) (h m s)	Dec. (1950.0) (° ′ ″)	$S^{330\ MHz}$ peak/total[a] (Jy beam^{-1}/Jy)	rms (mJy/beam)	No. of antennas	uv range min/max ($k\lambda$)	PBAF	Other Names
G5.4 − 1.2	17 58 30	− 24 49 00	4.0/37.5	120	22	0.05/1.13	1.00	Milne 56
G6.4 − 0.1	17 58 33	− 23 24 59	17.3/660	400	22	0.03/1.12	1.14	W28
G11.2 − 0.3	18 08 30	− 19 26 00	22.3/39.0	200	22	0.03/1.14	1.09	
G11.4 − 0.1	18 07 47	− 29 06 00	4.2/17.6	150	22	0.03/1.14	1.00	
G12.0 − 0.1	18 09 12	− 18 37 59	2.7/7.8	125	22	0.03/1.14	1.10	
G18.8 + 0.3	18 21 18	− 12 27 59	6.3/55.3	200	15	0.04/1.13	1.64	Kes 67
G21.5 − 0.9	18 30 46	− 10 35 59	6.6/9.3	150	22	0.03/1.15	2.15	
G21.8 − 0.6	18 30 17	− 10 14 00	14.0/132.2	200	22	0.03/1.15	1.41	Kes 69
G22.7 − 0.2	18 31 10	− 09 09 59	2.5/84.4	200	22	0.03/1.15	1.22	
G23.3 − 0.3	18 31 22	− 08 51 58	6.9/151.0	200	22	0.03/1.15	1.50	W41
G29.7 − 0.3	18 43 48	− 03 01 59	18.1/27.4	600	22	0.03/1.14	3.30	Kes 75
G30.7 + 1.0	18 41 16	− 01 32 00	2.6/8.6	175	15	0.05/1.12	1.29	
G31.9 + 0.0	18 46 48	− 00 58 00	21.9/44.8	300	22	0.03/1.14	1.90	3C391
G32.8 − 0.1	18 48 48	− 00 03 00	3.4/31.3	300	22	0.03/1.14	1.67	Kes 78
G33.6 + 0.1	18 50 00	+ 00 36 00	8.3/34.8	300	22	0.03/1.14	1.13	Kes 79
G34.7 − 0.4	18 53 44	+ 01 27 00	17.0/469	400	22	0.03/1.14	1.83	W44/3C392
G36.6 − 0.7	18 58 36	+ 02 50 00	0.6/6.7	100	22	0.03/1.15	1.18	
G39.2 − 0.3	19 01 35	+ 05 22 58	14.6/42.5	400	22	0.03/1.15	2.71	3C396
G41.1 − 0.3	19 05 09	+ 07 04 00	22.3/46.3	250	22	0.03/1.15	1.15	3C397
G49.2 − 0.7	19 20 45	+ 14 10 00	12.0/336[b]	100	22	0.04/1.14	1.02	W51

[a] See notes to individual sources (Sec. 3) for details regarding flux density measurements for SNRs in complex regions.
[b] Integrated flux density includes contributions from both thermal and nonthermal emitting regions.

Both flux density and phase calibration were based directly on observations of 3C286, 3C380, and 3C48 which were defined to have flux densities at 330 MHz of 29, 45, and 47 Jy, respectively. These values are consistent with the Baars *et al.* (1977) absolute flux density scale whose intrinsic uncertainty at these long wavelengths is at least 10%. Standard computer programs were used to interpolate the gain and phase of the instrument between calibrator observations. These procedures are normal for the VLA and are thought to provide a flux density calibration which is consistent to a few percent with possible systematic errors of up to ~5%, or less than the intrinsic errors in the absolute flux density scale. For a more detailed description of the VLA see Napier *et al.* (1983). For the flux densities presented in this paper, errors due to instrumental uncertainties and errors introduced while obtaining flux densities for poorly defined sources are expected to dominate, and these are discussed in more detail in Sec. *3.1* below.

The shortest array spacings at 90 cm were typically ~30λ, but varied from source to source. This means that in general sources larger than ~30′ at 90 cm may be undersampled and have their flux densities underestimated by > ~10%. (Table 1 lists the precise uv range available for each source.) The individual uv datasets, after calibration, correction, and inspection for quality, were combined to produce a single visibility dataset for each pointing position. These data were then Fourier transformed to produce "dirty" maps which were then CLEANed and restored with elliptical Gaussians. The final maps presented in Sec. 3 below, after correction for primary beam attenuation, are subimages obtained from these CLEANed fields. The measured rms noise levels vary from map to map, but are generally in the range of ~200–400 mJy beam^{-1}.

We note several problems which adversely affected the quality of the data. First, cross-talk between individual antennas often contaminated up to ~25% of the data on the shortest ($<0.2k\lambda$) baselines. These bad visibilities could usually be identified by their unusually large amplitudes or by their correspondence with unrealistic artifacts in the transformed images (e.g., broad stripes). These data were eliminated if possible, and were most severe during the March 1987 observations from which data for only two sources were obtained. Second, in principle a three-dimensional Fourier transform is required to properly image the large field of view provided by a noncoplanar array at low frequencies, and our data were reduced using a two-dimensional FFT reduction package. The effects of this error on the quality of the images is small when the array is in the D configuration, and are not expected to have a significant effect on our D array maps (Perley & Cornwell 1991). The error introduces a distortion which increases radially from the phase center. Serious errors arise when the product of the angular offset of the source in radians from the phase center multiplied by this same offset in synthesized beams exceeds unity. This condition is not violated for any of the data presented in this paper.[2] Furthermore, while the effect may distort the appearance of point sources far (>1°) from the phase center (and similarly fine details in the brightness structure of extended emission), it appears to have little effect on integrated flux densities (Uson *et al.* 1991). Finally, uncertainties related to the focal properties of the early *P*-band observing system (e.g., pointing characteristics) used to obtain the data presented here may have led to systematic errors on dirty maps which are not completely corrected by the CLEANing process. This is reflected in higher than theoretical noise levels on the final maps.

Despite these known sources of errors, the integrated flux densities and the sensitivity to extended structure for the sources we present here are among the best currently available at low frequencies. (See Sec. *3.1* for a discussion of estimated errors for integrated flux densities.) However, these data cannot provide high dynamic range imaging of fine details in the surface-brightness distributions of these SNRs. Such information is better provided by the much improved,

[2] For a nominal 3′ beam this condition is met at a distance of ~100′ from the phase center, corresponding to a Primary Beam Attenuation Factor (PBAF) of 5.2. The average distance from the phase center for the 20 SNRs imaged in this paper is ~30′, corresponding to an average PBAF of 1.52.

currently available 27 antenna *P*-band VLA system, and by observations in wider array configurations employing full three-dimensional imaging techniques.

3. RESULTS

The 90 cm images of 20 previously identified Galactic SNRs are shown in Figs. 1–19. (There are only 19 images since G22.7 − 0.2 and G23.3 − 0.3 appear on the same map.) In some cases the images are confused by other sources (often previously identified H II regions), and these are discussed below in the notes which apply to individual fields. Table 1 summarizes the measurements obtained from the maps, and the columns contain the following information:

Column 1: The name of the source in the standard Galactic notation as they appear in the most recent Green (1991) Galactic SNR catalog.

Columns 2 and 3: Position of maximum in right ascension and declination (epoch 1950.0). Note that for most SNRs the position of maximum intensity is rarely coincident with the morphological center of the source.

Column 4: The peak and total 90 cm (330 MHz) flux density in units of Jy/beam and Jy, respectively. Integrated flux densities were determined using AIPS tasks IMFIT and TVSTAT, with boundaries for the region of integration generally determined by eye. No attempt was made to remove other than a uniform background unless otherwise noted under the notes to individual sources in Sec. *3.2*.

Column 5: The rms noise in the map in units of mJy/beam.

Column 6: The number of *P*-band antennas available for the observations.

Column 7: The minimum and maximum available uv range used to map the source in units of $k\lambda$.

Column 8: The primary beam attenuation factor (PBAF) at the position of maximum flux density.

Column 9: Other commonly used names for the sources. Abbreviations have the following definition:

(i) W—Source appears in the Westerhout survey at 1390 MHz (Westerhout 1958).

(ii) 3C—Source appears in the Cambridge 3C catalog (Bennett 1963).

(iii) Kes—Source appears in the Kesteven survey at 408 MHz (Kesteven 1968).

3.1 Uncertainties in Integrated Flux Densities

Errors in the integrated flux densities are expected to arise mainly from the following sources: (1) the inherent rms noise in the map; (2) the uncertainty in the primary beam correction;[3] (3) systematic errors associated with obtaining integrated flux densities for extended sources in confused fields; and (4) the error associated with the absolute flux density calibration. (Errors associated with the problems of cross-talk and wide-field imaging, discussed in Sec. 2 above, are reflected in an increase in the rms noise.) In general, we found that the effects due to (1) and (3) dominate, particularly for weak, poorly defined sources with low surface brightness. Based on these considerations, we estimate an error of 20% in integrated flux density or 2 Jy, whichever is greater, for sources observed in 1988 when 22 antennas were available, and 30% in integrated flux density for the fields observed in 1987 when only 15 antennas were available. (Table 1, Column 6 lists the number of antennas available for each SNR observed.)

3.2 Extended Notes on Individual Sources

G5.4 − 1.2. Our observations, shown in Fig. 1, confirm the flat spectrum of emission ($\alpha \sim -0.2$) seen for this complicated source at higher frequencies. This favors an interpretation of the source as mainly plerionic, although it has also been suggested that it may be a composite (Weiler & Sramek 1988; Green 1991). The mildly flat spectrum we see could easily be a blend between flatter spectrum ($\alpha \sim 0.0$) plerionic emission and steeper spectrum shell emission. Caswell *et al.* (1987) suggest a shell, but we do not find any evidence for the low surface-brightness eastern shell which their 843 MHz MOST map shows. Either it is thermal, has a flat spectrum atypical of shell emission, or we have insufficient surface-brightness sensitivity to detect it.[4] The powerful source to the northeast is the thermal source associated with the Lagoon Nebula (M8). It is now believed that a fast, young, and potentially very high velocity pulsar is associated with a wind blow nebula near the western edge of the SNR, supporting the interpretation that the remnant is at least partially plerionic (Frail & Kulkarni 1991; Manchester *et al.* 1991). The integrated flux density of 37.5 Jy we list in Table 1 does not include the contribution from the emission south of $\sim -25°10'$, which may be unrelated to the SNR.

G6.4 − 0.1. This is a well known SNR exhibiting bright shell-type emission from a nonthermal ring and possibly plerionic emission from a flat spectrum core; thus it is classified as a composite in Green's (1991) catalog. A compact x-ray source near the center supports the case for a plerionic component (Andrews *et al.* 1983). Recombination line observations have shown that compact H II regions lie along the line of sight, but this emission would probably be optically thick and contribute little relative flux at our frequency (Andrews *et al.* 1985). Our map shown in Fig. 2, is dominated by the extended nonthermal emission of ~660 Jy which together with Green's estimate of its flux at 1 GHz gives an overall spectral index of $\alpha \sim -0.7$. This shows that the steeper spectrum shell emission dominates over any plerionic or thermal emission at low frequencies. Our map shows considerable extended low surface-brightness emission associated with the interior of the bright shell which is difficult to distinguish from the Galactic background on higher frequency single-dish maps (e.g., see Reich *et al.* 1990; Altenhoff *et al.* 1978). The bright extended source to the south near $\delta = -24°5'$ is a known H II region appearing in Lockman's (1989) latest catalog.

G11.2 − 0.3. This source is a shell-type SNR which is only marginally resolved at our resolution, and our map is shown in Fig. 3. Previous observations (see Morsi & Reich 1987a, and references therein) suggest a flatter spectrum core which would contribute relatively little flux on our map. Our integrated flux density is consistent with the typical shell-type spectrum of $\alpha \sim -0.5$ indicated by previous observations (Green 1991; Kassim 1989a). Green *et al.* (1988) de-

[3] This uncertainty varies from ~2% for sources 10′ from the phase center to > 10% for sources > 80′ from the phase center.

[4] Unfortunately, even if the eastern shell had an $\alpha = -0.5$ shell-type spectrum, it would appear at only the 2–3σ level above the noise on our 90 cm VLA map. Observations with the presently available improved and more sensitive VLA *P* band are warranted to set more meaningful limits on the nondetection.

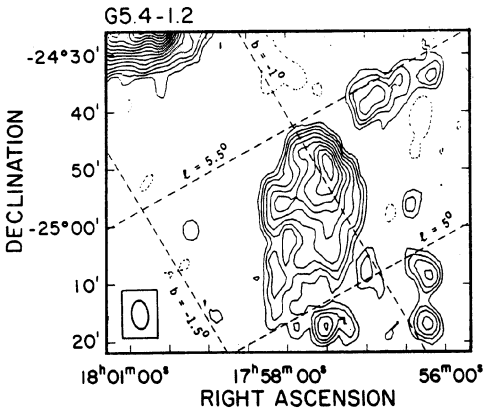

FIG. 1. Contour map of G5.4 − 1.2. HPBW is 296″ × 178″ at P. A. + 5° and is shown at the lower left. Peak flux is 6.8 Jy/beam, and the rms noise σ is ≈120 mJy/beam. Contours are at (− 3, 3, 5, 7, 10, 14, 18, 22, 26, 30, 34, 38, 42, 46, 50, and 54) *σ.

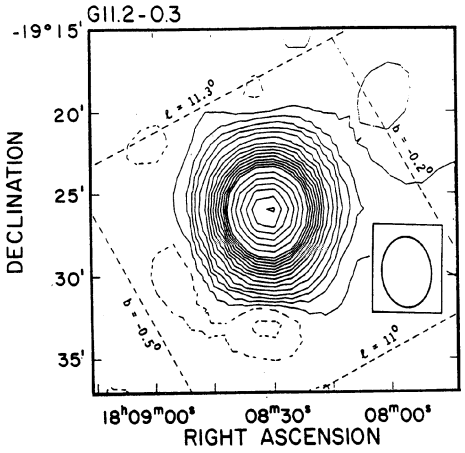

FIG. 3. Contour map of G11.2 − 0.3. HPBW is 247″ × 189″ at P.A. + 3.5° and is shown at the lower right. Peak flux is 22.3 Jy/beam and the rms noise σ is ≈200 mJy/beam. Contours are at (− 3, − 1, 3, 5, 7, 10, 14, 18, 22, 26, 30, 34, 38, 42, 46, 50, 60, 70, 80, 90, 100, 110, and 120) *σ.

scribe this source as an "evolved Cassiopeia A" based on high resolution VLA observations.

G11.4−0.1. This source is probably a shell-type SNR. Our integrated flux density of ∼18 Jy, derived from our image shown in Fig. 4, together with higher frequency measurements indicates a steeper spectrum of $\alpha \sim -0.7$ than the $\alpha = -0.5$ listed in Green's (1991) catalog. Previous low frequency flux density measurements were uncertain due to contamination by the sidelobes of a nearby source, which could explain the uncertainty in the derived spectrum (e.g., see Clark *et al.* 1975).

G12.0−0.1. Our map, shown in Fig. 5, reveals emission from a northeastern and southwestern component, but only the former centered near $\alpha = 18^h09^m15^s$, $\delta = -18°37.5'$ has been considered the SNR. Furthermore, even this brighter northeastern component is known to consist of an eastern nonthermal component and a western thermal component which are not well resolved at our resolution (Clark *et al.* 1975). Clark *et al.* estimate the thermal contribution at 408 MHz to be ∼3 Jy, which should be a reasonable upper limit to the 330 MHz thermal flux density. We measure a total flux of ∼7.8 Jy from the northeastern component, implying a lower limit of ∼4.8 Jy of nonthermal flux. Combined with the 6 cm Clark *et al.* flux density listed in Green's catalog, this implies $\alpha < -0.5$ which is compatible with existing estimates of the spectrum. However, our map suggests that the SNR is larger than previously realized, and if the southeastern component near $\alpha = 18^h08^m40^s$, $\delta = -18°45'$ completes the shell of a single larger SNR, we find an integrated flux density of > 11.6 − 3 or > 8.6 Jy for

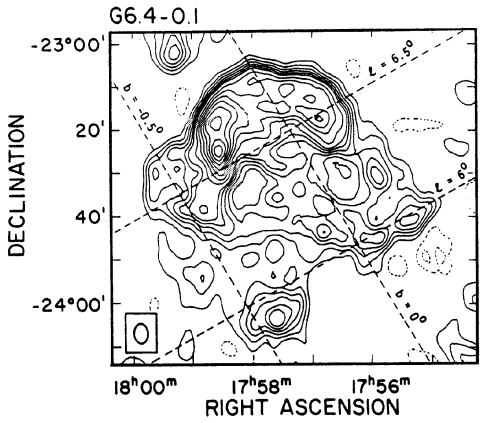

FIG. 2. Contour map of G6.4 − 1.2. HPBW is 265″ × 184″ at P.A. + 2° and is shown at the lower left. Peak flux is 17.3 Jy/beam and the rms noise σ is ≈400 mJy/beam. Contours are at (− 4, − 2, 2, 4, 6, 8, 10, 12, 16, 20, 24, 28, 32, 36, 40, 44, and 48) *σ.

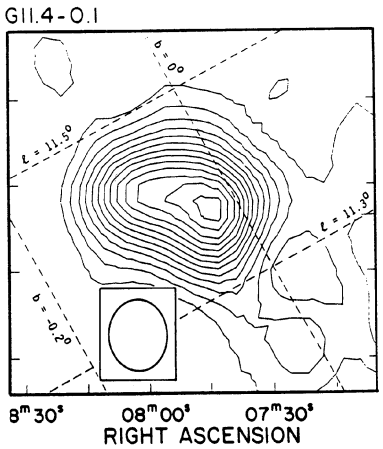

FIG. 4. Contour map of G11.4 − 0.1. HPBW is 247″ × 189″ at P. A. + 3.5° and is shown at the lower left. Peak flux is 4.2 Jy/beam and the rms noise σ is ≈150 mJy/beam. Contours are at (− 1, 3, 5, 7, 9, 11, 13, 15, 17, 19, 21, 23, 25, 27, and 29) *σ.

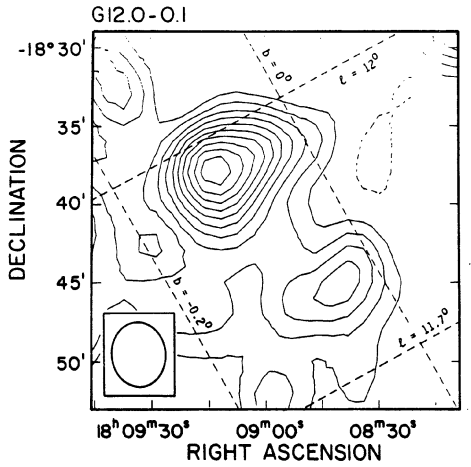

FIG. 5. Contour map of G12.0 − 0.1. HPBW is 247″ × 189″ at P.A. + 3.5° and is shown at the lower left. Peak flux is 2.7 Jy/beam and the rms noise σ is ≈125 mJy/beam. Contours are at (− 4, − 2, 2, 4, 6, 8, 10, 12, 14, 16, 18, 20, 22, 24, 26, 28, 30, 32, 34, 36, 38, and 40) *σ.

the entire source. If considered a single larger shell, the source exceeds 20′ in extent.

G18.8+0.3. The integrated flux density of this source, derived from our map shown in Fig. 6, is ∼55 Jy. This is significantly larger than the ∼37 Jy expected based on the $\alpha = -0.3$ spectral index and 1 GHz flux listed in Green's catalog. But our measurement is consistent with the $\alpha = -0.5$ shell-type spectrum derived by Kassim (1989a). We favor the steeper intrinsic spectrum, but it is possible that our 330 MHz flux density includes contributions from unrelated, small diameter sources near the northwest and southern extensions of the source. The presence of these superimposed sources and their possible confusing effects on the derived spectrum has been noted earlier (Clark *et al.* 1975).

If the extension near $\alpha = 18^h 20^m 35^s$, $\delta = -12°28'$ is not part of the SNR our integrated flux is ∼50 Jy.

G21.5−0.9. This is a well-known plerionic SNR which has been observed extensively, particularly at higher frequencies (> 10 GHz) where an apparent turnover is seen in the continuum spectrum (Salter *et al.* 1989). In the 1–10 GHz range the spectrum is flat ($\alpha \sim 0.0$) and the flux density is ∼6 Jy, but below 1 GHz there are indications, including our 330 MHz measurement of ∼9 Jy from our map shown in Fig. 7, that the spectrum becomes steeper at lower frequencies. One possibility is that in addition to the plerionic component, there may be associated weak, steeper spectrum shell-type emission which would have been easily missed by higher frequency measurements. Higher low frequency flux densities have also been recorded by other observers [e.g., see Kassim (1989a) for a review of low frequency flux measurements]. Higher resolution 330 MHz VLA observations are needed to determine whether the source may be a composite, or whether the low frequency flux densities may be contaminated by one or more nonthermal, steep-spectrum background sources. If the first possibility holds true, the source may warrant reclassification as a composite type SNR. [Note: The source appears slightly resolved at our resolution while observations made above 1 GHz indicate that it should not be (Morsi & Reich 1987b). This might indicate the presence of extended shell emission, but we consider it marginal evidence since the apparent extended structure may only be a distortion introduced by the imaging errors discussed in Sec. 2 above. After G29.7 − 0.3 and G39.2 − 0.3, this source had the greatest distance (71′) from the phase center.]

G21.8−0.6. This source shows the typical, incomplete shell morphology of many Galactic SNRs. Our map is shown in Fig. 8. The integrated flux density at 330 MHz of 118 Jy is, within the errors, completely compatible with the $\alpha = -0.5$ spectral index and 1 GHz flux density estimate listed in Green's catalog. The nearby source at $\alpha = 18^h 29^m 45^s$, $\delta = -10°$ is a cataloged H II region presumably unrelated to the SNR.

G22.7−0.2. This is a fairly complete shell-type SNR in a

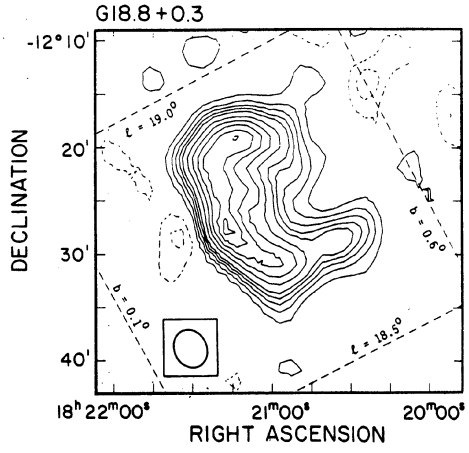

FIG. 6. Contour map of G18.8 + 0.3. HPBW is 208″ × 174″ at P.A. + 22° and is shown at the lower left. Peak flux is 6.3 Jy/beam and the rms noise σ is ≈200 mJy/beam. Contours are at (− 4, − 2, 2, 4, 6, 8, 10, 14, 18, 22, 26, 30, and 34) *σ.

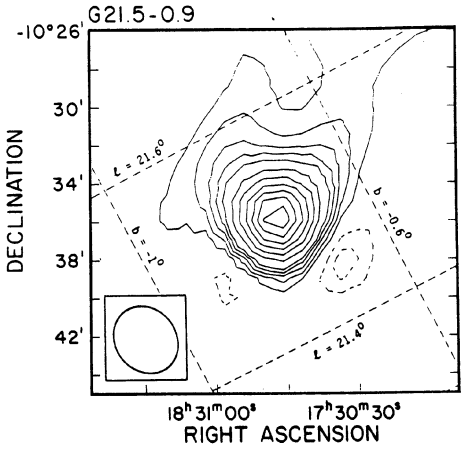

FIG. 7. Contour map of G21.5 − 0.9. HPBW is 206″ × 198″ at P.A. 34° and is shown at the lower left. Peak flux is 6.6 Jy/beam and the rms noise σ is ≈150 mJy/beam. Contours are at (− 4, − 2, 2, 4, 6, 8, 10, 15, 20, 25, 35, and 40) *σ.

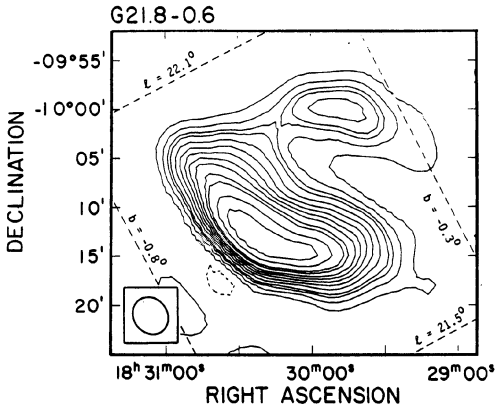

FIG. 8. Contour map of G21.8 − 0.6. HPBW is 209″ × 198″ at P.A. 34° and is shown at the lower left. The peak flux is 14.0 Jy/beam and the rms noise σ is ≈200 mJy/beam. Contours are at (− 2, 2, 5, 8, 10, 14, 18, 22, 26, 30, 36, 40, 50, 60, 70, and 80) *σ.

complex region whose flux density is somewhat uncertain due to its overlap with the SNR G23.3 − 0.3 and the contribution from at least one superimposed H II region. Our image of both SNRs is shown in Fig. 9. Assuming a base level of ~1 Jy/beam we estimate the contribution from the known H II region near $\alpha = 18^h 31^m 45^s, \delta = -9°18'$ to be only ~1 Jy if it is unresolved. With a total flux of ~83 Jy for the SNR + H II region, we estimate ~82 Jy of emission from the SNR. This flux density gives a spectral index of $\alpha \sim -0.8$ when combined with the 1 GHz estimate in Green's catalog, unusually steep for even a shell-type SNR [Green's (1991) catalog lists $\alpha = -0.6$]. We suspect that our 330 MHz flux density is an overestimate due to confusion with G23.3 − 0.3 and any extended thermal emission associated with the H II region. The source is roughly circular and has an angular diameter of ~30′.

G23.3 − 0.3. This source, also shown in Fig. 9, is an asymmetric shell in a complex region whose flux density is difficult to estimate because of its near overlap with the SNR G22.7 − 0.2, and the superposition of at least two small diameter H II regions. Assuming a baselevel of 2.7 Jy/beam we estimate the contribution from the known H II regions near $18^h 32^m, \delta = -8°35'$ and $18^h 32^m, \delta = -8°43'$ to be 3.4 and 1.8 Jy, respectively, if they are unresolved at our resolution. We find a total flux of 143 Jy for SNR + H II regions, indicating ~138 Jy of emission from the SNR. This gives a spectral index $\alpha = -0.6$ based on the 1 GHz flux estimate in Green's catalog, only slightly steeper than the $\alpha = -0.5$ listed there. As with G22.7 − 0.2, if any of the H II regions are extended, our value of the SNR flux would be an overestimate, and could easily account for the slightly steeper spectrum indicated by our measurements.

G29.7 − 0.3. This is a bright SNR that has been observed over a wide range of frequencies. Our map is shown in Fig. 10. Although it appears marginally resolved at our resolution, we do not consider this significant since it lies significantly further (88′, see Table 1) from the phase center than any other source in our study, and thus its shape may be distorted by the errors related to this discussed in Sec. 2 above. High resolution, high frequency observations reveal a flat spectrum core, while the low frequency measurements are dominated by steeper spectrum shell emission. Thus it is probably a composite type SNR. Our 330 MHz integrated flux density implies a slightly steeper spectral index of $\alpha = -0.8$ than the $\alpha = -0.7$ listed in Green's catalog based on his estimate of the flux at 1 GHz, but the results agree within the errors of our measurement. If the source is a composite, one would expect the overall spectral index to be flatter at higher frequencies where the plerionic component is relatively stronger, and that the total spectrum would steepen at lower frequencies where the shell-emission dominates.

G30.7 + 1.0. This is an SNR of unknown morphological type, although Reich *et al.* (1986) find a constant spectral index distribution across the source as is usually the case for extended shell-type SNRs. Our integrated flux is consistent with the $\alpha \sim -0.4$ spectral index and higher frequency flux densities listed by Reich *et al.* (1986) and in Green's (1991) catalog. The peak of our map, shown in Fig. 11, corresponds

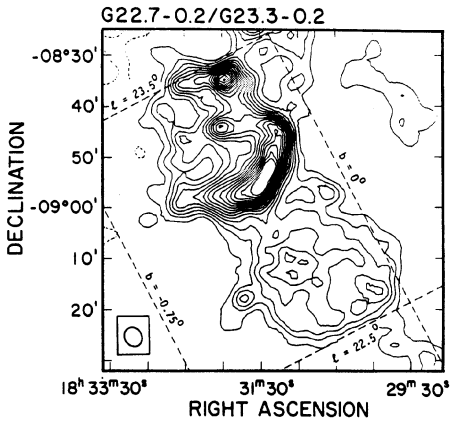

FIG. 9. Contour map of G22.7 − 0.2 and G23.3 − 0.3. HPBW is 206″ × 198″ at P.A. 34° and is shown at the lower left. The peak flux is 6.9 Jy/beam and the rms noise σ is ≈200 mJy/beam. Contours are at (− 4, − 2, 2, 4, 6, 8, 10, 12, 14, 16, 18, 20, 22, 24, 26, 28, and 30) *σ.

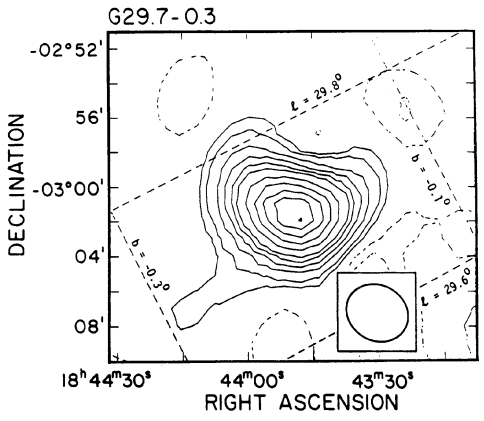

FIG. 10. Contour map of G29.7 − 0.3. HPBW is 222″ × 205″ at P.A. + 62° and is shown at the lower right. Peak flux is at 18.1 Jy/beam and the rms noise σ in the map is ≈600 mJy/beam. Contours are at (− 2, − 1, 1, 2, 4, 6, 8, 10, 14, 18, 22, 26, 30, and 34) *σ.

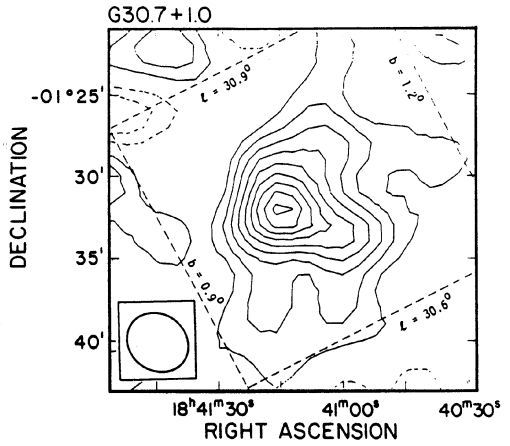

FIG. 11. Contour map of G30.7 + 1.0. HPBW is 231″ × 213″ at P.A. + 51° and is shown at the lower left. The peak flux is 2.6 Jy/beam and the rms noise σ in the map is ≈275 Jy/beam. Contours are at (− 2, − 1, 1, 2, 3, 4, 5, 6, 7, 8, 9, 10, and 11) *σ.

with the unresolved component seen in the 5 GHz map of Reich *et al.* (1986). It is unclear whether this source is associated with the SNR, but it appears to have a similar nonthermal spectrum to the extended emission. Our results confirm this, since this small diameter component would produce an excess low frequency flux if it had a spectrum much steeper than the $\alpha = -0.4$ spectrum of the extended emission. Higher resolution observations are needed to determine the nature of the small-diameter component.

G31.9+0.0. This is a shell-type SNR which appears as an incomplete shell at higher frequencies but is only marginally resolved at our resolution. Our map is shown in Fig. 12. Our integrated flux density is consistent with the $\alpha = -0.55$ shell-type spectral index and estimated 1 GHz flux density listed in Green's catalog.

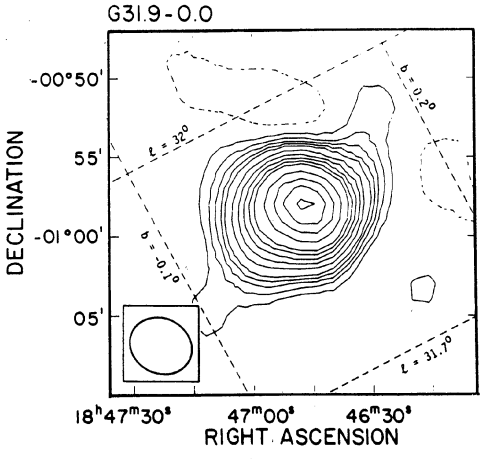

FIG. 12. Contour map of G31.9 + 0.0. HPBW is 222″ × 205″ at P.A. 62° and is shown at the lower left. The peak flux is 21.9 Jy/beam and the rms noise σ in the map is ≈300 mJy/beam. Contours are at (− 2, 2, 4, 6, 8, 10, 14, 18, 22, 26, 30, 40, 50, 60, 70, 80, and 90) *σ.

G32.8−0.1. This is a poorly defined source in a confused region. Our 330 MHz map, shown in Fig. 13, shows good agreement with the 408 MHz map presented by Caswell *et al.* (1975), but our integrated flux density of ~32 Jy is significantly larger than the 12.8 Jy they report at the relatively nearby frequency. If we combine our measurement with the ~8 Jy flux density reported by Caswell *et al.* (1975) at 5000 MHz, we derive the typical shell-type spectral index $\alpha = -0.5$, which is consistent with the shell-like morphology revealed in the low frequency maps. Green's catalog lists an uncertain $\alpha = -0.2$? based on the Caswell *et al.* result which they state is uncertain. We favor the $\alpha = -0.5$ spectrum based on our new low frequency flux density measurement and the apparent shell-like morphology. The shell is elongated north–south and extends ~25′ in declination. The strong source just off the map to the northeast is a cataloged H II region, and the source near $\alpha = 18^h48^m10^s$, $\delta = -00°23'$ is a weak feature we have not included in our flux density integration for the SNR.

G33.6+0.1. This is another SNR located in a complex region, and is identified as a shell-type remnant in Green's catalog. The small-diameter source near $\alpha = 18^h49^m15^s$, $\delta = +00°32'$ appearing on our map shown in Fig. 14, was once thought to be a new class of radio star possibly associated with SNRs (Ryle *et al.* 1978). Follow-up observations of this source have indicated that it is unlikely to be associated with G33.6 − 0.1 and is probably extragalactic (e.g., see Seaquist & Gilmore 1982; Van Gorkom *et al.* 1982, and references therein.) This result has been recently confirmed through H I absorption measurements by Frail & Clifton (1989). Our integrated flux combined with the 1 GHz flux estimated from Green's (1991) catalog indicates a slightly flatter spectral index of $\alpha = -0.4$ than the $\alpha = -0.5$ listed there. However examination of the wide scatter in the low frequency data listed in Kassim (1989a) reflect considerable confusion in earlier measurements, perhaps due to confusion by the unrelated point source. Our map, albeit with limited angular resolution, shows a centrally condensed morphology also reflected in maps made at higher frequencies (Caswell *et al.* 1981; Frail & Clifton 1989). Higher resolution radio observations and x-ray observations (Velusamy *et al.* 1991) suggest that the peaked emission near $\alpha = 18^h50^m$,

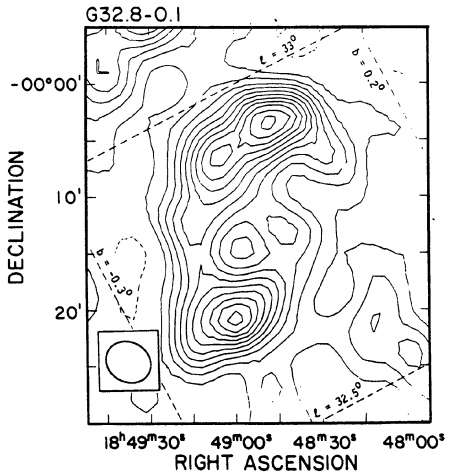

FIG. 13. Contour map of G32.8 − 0.1. HPBW is 227″ × 213″ at P.A. + 57°, and the rms noise σ in the map is ≈300 mJy/beam. Contours are at (− 2, − 1, 1, 2, 3, 4, 5, 6, 7, 8, 9, 10, and 11) *σ.

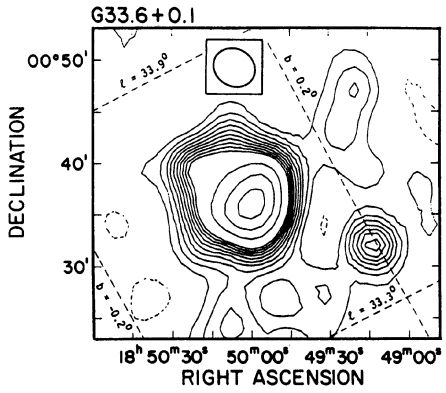

FIG. 14. Contour map of G33.6 + 0.1. HPBW is 227″ × 213″ at P.A. + 57°, and the rms noise σ in the map is ≈300 mJy/beam. Contours are at (− 1, 1, 2, 3, 4, 5, 6, 7, 8, 9, 10, 15, 20, 25, 30, 35, 40, 45, and 50) *σ.

$\delta = 00°35'$ may be plerionic, which would indicate that the remnant may be a composite. The weak feature near $18^h49^m20^s$, $\delta = 00°48'$ is probably not related to the SNR and was not included in the integrated flux listed in Table 1.

G34.7 − 0.4. This very bright source appears quite striking even on low frequency maps because of its large angular size (∼45′), and it has previously been considered a classic shell-type SNR. However, Wolszczan *et al.* (1991) have recently discovered a 267 ms pulsar (PSR 1853 + 01, located near $\alpha = 18^h53^m28^s$, $\delta = 01°09'23''$) within the shell of G34.7 − 0.4 which they argue is physically associated with the SNR. If this suggested SNR/pulsar association is confirmed, it might warrant reclassification of the remnant as a composite. We find no apparent evidence on our image shown in Fig. 15 for either the pulsar or plerionic emission which may be associated with it.

Our derived integrated flux density of 469 Jy gives a steeper spectral index $\alpha = -0.6$ than the $\alpha = -0.3$ listed in Green's catalog, when referenced to his estimate of the 1 GHz flux density. But again there is a very large scatter in the published flux densisities, particularly at the low frequencies. For example, Clark *et al.* (1975) find $S_{408} = 299$ Jy while Kesteven (1968) found $S_{408} = 390$ Jy with the same Molonglo telescope. By comparison Dickel & DeNoyer (1975) found $S_{430} = 540$ Jy with the Arecibo telescope. If we take our 330 MHz flux density and combine it with the old but presumably reasonably well determined 10.7 MHz flux density of 105 Jy (Kundu & Velusamy 1972), we find $\alpha = -0.4$. We favor a spectral index between − 0.3 and − 0.4, which would be compatible with the spectral index expected from a composite. It is surprising that the flux density of such a bright source should be so poorly determined. We suggest that because of its large angular size, many early interferometric observations may have had too poor uv coverage to accurately measure its total power.

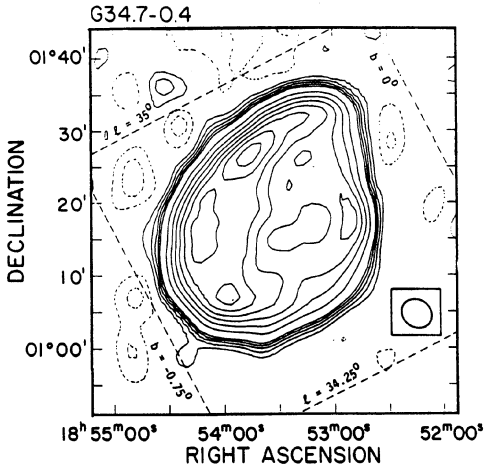

FIG. 15. Contour map of G34.7 − 0.4. HPBW is 227″ × 213″ at P.A. + 57°, and the rms noise σ in the map is ≈400 mJy/beam. Contours are at (− 2, − 1, 1, 2, 3, 4, 5, 10, 15, 20, 25, 30, 35, 40, 45, and 50) *σ.

G36.6 − 0.7. This is a recently identified SNR located in a very complex region. Fürst *et al.* (1987) observed a polarized arc of emission on which the SNR identification was based, and this arc is clearly seen on our 330 MHz map. Fürst *et al.* do not list an integrated flux density due to confusion with nearby sources that may not be part of the SNR. We calculate a brightness temperature spectral index $\beta = -2.4$ (where $T\alpha\nu^{+\beta}$) for the arc, by comparison of our 330 MHz map, shown in Fig. 16, with the Fürst *et al.* 4750 MHz map. Our calculation was for the region near the relatively unconfused but well-extended component with a peak near $18^h58^m40^s$, $\delta = 02°50'$. This brightness temperature spectral index corresponds to an $\alpha = -0.4$ flux density spectral index, supporting the conclusion by Fürst *et al.* that this feature at least is probably part of a SNR. Further observations are certainly needed to better estimate the parameters for this source. If the bright, small-diameter component near $\alpha = 18^h59^m$, $\delta = 02°41'$ is part of the SNR, the integrated flux for the entire region of extended emission on our map (extending nearly 30′ north–south) is ∼9.9 Jy. The integrated flux we list in Table 1 (∼6.7 Jy) does not include the contribution from this small-diameter feature or from extended emission south of $\sim\delta = 02°35'$.

G39.2 − 0.3. This is a shell-type SNR which is only marginally resolved with the D array. It has been observed over a wide range of frequencies, including higher resolution observations at 327 MHz by Patnaik *et al.* (1990). From their

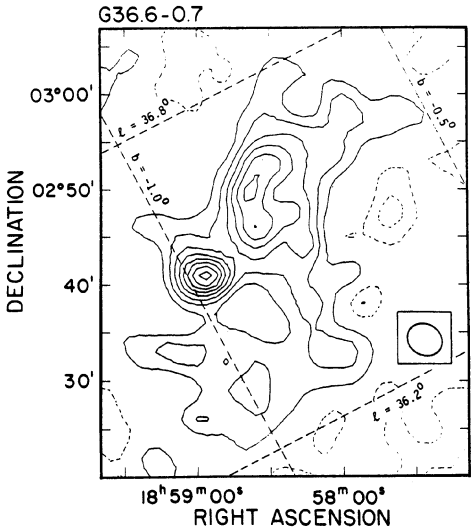

FIG. 16. Contour map of G36.6 − 0.7. HPBW is 222″ × 202″ at P.A. + 61°, and the rms noise σ in the map is ≈100 mJy/beam. Contours are at (− 2, − 1, 1, 2, 3, 4, 5, 6, 7, 8, 9, 10, 20, 30, 40, 50, 60, 70, and 80) *σ.

own measurements and from those present in the literature, they derive a spectrum with an index of $\alpha = -0.4$, and a flux density at 327 MHz of 28 Jy. In our study, this source was the second farthest (after G29.7 − 0.3) from the phase center of any other SNR (see Table 1), and was located in an area with a confused background. Our map is shown in Fig. 17. We fit an elliptical Gaussian to the source with a zero level and slope. Our integrated flux of ~24 Jy is remarkably consistent with the Patnaik *et al.* measured $S_{327} = 23.5$ Jy and, within the errors, with their derived spectrum as well. Our map shows a weak extension to the southwest which may correspond to a small-diameter feature seen on their VLA D-array map at 1465 MHz, but for which there is only marginal evidence on their 327 MHz image. However, we regard features at this level to be of marginal significance on our map because of the confused background, and the errors related to the unusually large distance from the phase center. Green lists $\alpha = -0.6$ for this source, but we favor the Patnaik *et al.* derived spectrum which is also consistent with the $\alpha = -0.4$ spectrum derived by Kassim (1989a).

G41.1−0.3. This source consists of two objects (Caswell *et al.* 1975), an H II region to the west and the SNR to the east, and they are only partially resolved at our resolution, as indicated by our map shown in Fig. 18. However our estimate of 38 Jy for the SNR alone is consistent, within the errors, of both the $\alpha = -0.4$ spectrum fit by Kassim (1989a) and the $\alpha = -0.48$ listed in Green's (1991) latest catalog.

G49.2−0.7. This is the well studied giant H II region/SNR complex known as W51. It is known to contain a complex superposition of nonthermal and thermal emitting regions, with the former assumed to be a Galactic SNR. Many of the small-diameter features on our map, shown in Fig. 19, correspond to positions from which recombination lines have been detected, while the extended emission is known to be at least partly nonthermal. The detection of x rays from this region (Seward 1990) strongly strengthens the SNR identification. A complete analysis of this source requires a consideration of observations over a wide range of frequencies, and will be presented separately (Odegard & Kassim 1992). A comparison of our integrated flux density for this complex with other published results is not meaningful here since we have made no attempt to disentangle the emission from the various overlapping features.

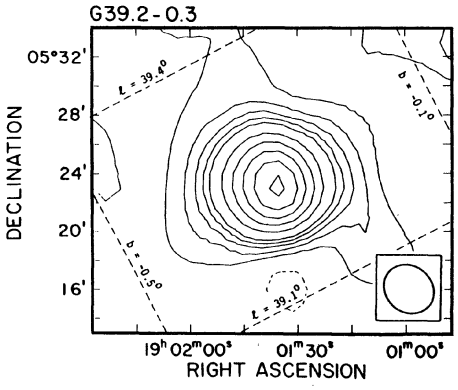

FIG. 17. Contour map of G39.2 − 0.3. HPBW is 217″ × 209″ at P.A. + 53°, and the rms noise σ in the map is ≈400 mJy/beam. Contours are at (− 2, 2, 4, 6, 8, 10, 15, 20, 25, 30, 35, 40, and 45) *σ.

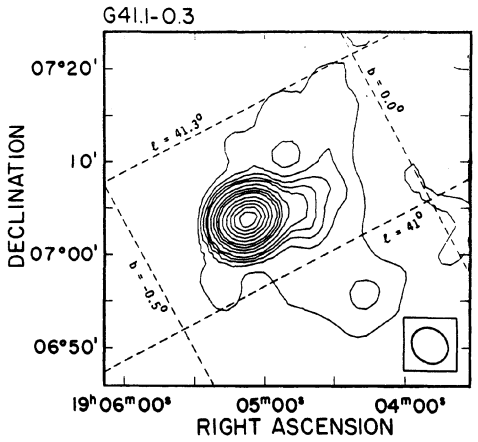

FIG. 18. Contour map of G41.1 − 0.3. HPBW is 217″ × 209″ at P.A. + 53°, and the rms noise σ in the map is ≈250 mJy/beam. Contours are at (− 1, 2, 4, 6, 8, 10, 15, 20, 25, 30, 40, 50, 60, 70, 80, 100, and 150) *σ.

4. CONCLUSIONS

We have presented 330 MHz VLA images and integrated flux densities for 20 previously identified Galactic SNRs. These data are useful for anchoring the intrinsic low frequency spectra of these sources, and the good surface-brightness sensitivity of the VLA in its D configuration can help establish the full extent of the nonthermal emission. Both can help establish the morphology of SNRs whose types are not well classified.

We have made only qualitative comparisons between parameters derived from our images and with information about these sources present in the literature. In several cases,

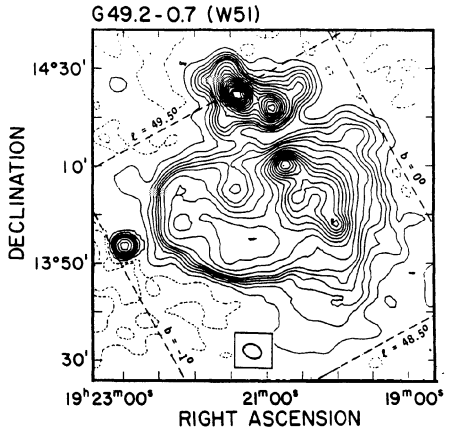

FIG. 19. Contour map of the giant H II region/SNR complex G49.2 − 0.7 (W51). HPBW is 209″ × 186″ at P.A. + 67°, and the rms noise σ in the map is ≈80 mJy/beam. Contours are at (− 4, − 2, 2, 6, 10, 14, 18, 22, 30, 40, 50, 60, 70, 80, 90, 100, 110, 120, 130, and 140) *σ.

we detect an excess of flux from that predicted by measurements made at higher frequencies. These discrepancies can be reconciled in the following three ways: (1) Higher frequency observations may have been insensitive to diffuse emission from extended sources due to the dynamic range limitation imposed on their surface-brightness sensitivity by the Galactic background; (2) higher frequency observations of composite SNRs are dominated by flat spectrum plerionic emission and would have been insensitive to low level steeper-spectrum shell-type emission if present; and (3) confusion on our 330 MHz images with extended thermal sources or steep-spectrum background (extragalactic) sources lying along the line of sight may have led us to overestimate some SNR flux densities. The effect of the first should be reduced at this lower frequency and comparison with currently available recombination line observations should have prevented confusion with obvious H II regions. However the last effect can become important at our lower frequency. The solution can be obtained by supplementing the observations presented here with higher resolution observations at the same frequency currently available with the VLA, or by other instruments now coming on-line with similar capabilities.

The author would like to thank the referee for several very useful comments and suggestions regarding the manuscript.

REFERENCES

Altenhoff, W. J., Downes, D., Pauls, T., & Schraml, J. 1978, A&AS, 35, 23
Andrews, M. D., Basart, J. P., Lamb, R. C., & Becker, R. H. 1983, ApJ, 266, 684
Andrews, M. D., Basart, J. P., & Lamb, R. C. 1985, AJ, 90, 310
Baars, J. W. M., Genzel, R., Pauliny-Toth, I. I. K., & Witzel, A. 1977, A&A, 61, 99
Bennett, A. S. 1963, MRAS, 127, 3
Caswell, J. L., Kesteven, M. J., Komesaroff, M. M., Haynes, R. F., Milne, D. K., Stewart, R. T., & Wilson, S. G. 1987, MNRAS, 225, 329
Caswell, J. L., Milne, D. K., & Wellington, K. J. 1981, MNRAS, 195, 89
Caswell, J. L., Clark, D. H., & Crawford, D. F. 1975, AuJPA, 37, 39
Clark, D. H., Caswell, J. L., & Green, A. J. 1975, AuJPA, 37, 1
Dickel, J. R., & DeNoyer, L. K. 1975, AJ, 80, 437
Frail, D. A., & Clifton, T. R. 1989, ApJ, 336, 854
Frail, D. A., & Kulkarni, S. R. 1991, Nature, 353, 785
Green, D. A. 1984, MNRAS, 209, 449
Green, D. A. 1988a, Ap&SS, 148, 3
Green, D. A. 1988b, in Lecture Notes in Physics, edited by W. Kundt (Springer, Berlin), Vol. 316, pp. 39–43
Green, D. A., Gull, S. F., Tan, S. M., & Simon, A. J. B. 1988, MNRAS, 231, 735
Green, D. A. 1991, PASP, 103, 209
Kassim, N. E. 1989a, ApJS, 71, 799
Kassim, N. E. 1989b, ApJ, 347, 915
Kassim, N. E., & Weiler, K. W. 1990a, Nature, 343, 146
Kassim, N. E., & Weiler, K. W. 1990b, ApJ, 360, 184
Kassim, N. E., Baum, S. A., & Weiler, K. W. 1991, ApJ, 374, 212
Kesteven, M. J. L. 1968, AuJPh, 21, 739
Kundu, M. R., & Velusamy, T. 1972, A&A, 20, 237
Lockman, F. J. 1989, ApJS, 71, 469
Manchester, R. N., Kaspi, V. M., Johnston, A. G., Lyne, A. G., & D'Amico, N. 1992, MNRAS (in press)
Morsi, H. W., & Reich, W. 1987a, A&AS, 71, 189
Morsi, H. W., & Reich, W. 1987b, A&AS, 69, 533
Napier, P. J., Thompson, A. R., & Ekers, R. D. 1983, Proc. IEEE, 71, 1295
Odegard, N. P., & Kassim, N. E. 1992, in preparation
Patnaik, A. R., Hunt, G. C., Salter, C. J., Shaver, P. A., & Velusamy, T. 1990, A&A, 232, 467
Perley, R. A. & Cornwell, T. J. 1991, in Radio Interferometry: Theory, Techniques, and Applications, ASP Conference Series, edited by T. J. Cornwell and R. A. Perley (ASP, Provo), Vol. 19, p. 184
Reich, W., Fürst, E., Reich, P., & Reif, K. 1990, A&AS, 85, 633
Reich, W., Fürst, E., Reich, P., Sofue, Y., & Handa, T. 1986, A&A, 155, 185
Ryle, M., Caswell, J. L., Hine, G., & Shakeshaft, J. 1978, Nature, 276, 561
Salter, C. J., Reynolds, S. P., Hogg, D. E., Payne, J. M., & Rhodes, P. J. 1989, ApJ, 338, 171
Seaquist, E. R., & Gilmore, W. S. 1982, AJ, 87, 378
Seward, F. D. 1990, ApJS, 73, 781
Uson, J. M., Bagri, D. S., & Cornwell, T. J. 1991, in Radio Interferometry: Theory, Techniques, and Applications, ASP Conference Series, edited by T. J. Cornwell and R. A. Perley (ASP, Provo), Vol. 19, p. 223
Van Gorkom, J. H., Goss, W. M., Seaquist, E. R., & Gilmore, W. S. 1982, MNRAS, 198, 757
Velusamy, T., Becker, R. H., & Seward, F. D. 1991, AJ, 102, 676
Weiler, K. W., & Sramek, R. A. 1988, ARA&A, 26, 295
Westerhout, G. 1958, Bull. Astr. Inst. Nether., 14, 215
Wolszczan, A., Cordes, J. M., & Dewey, R. J. 1991, ApJ, 372, L99

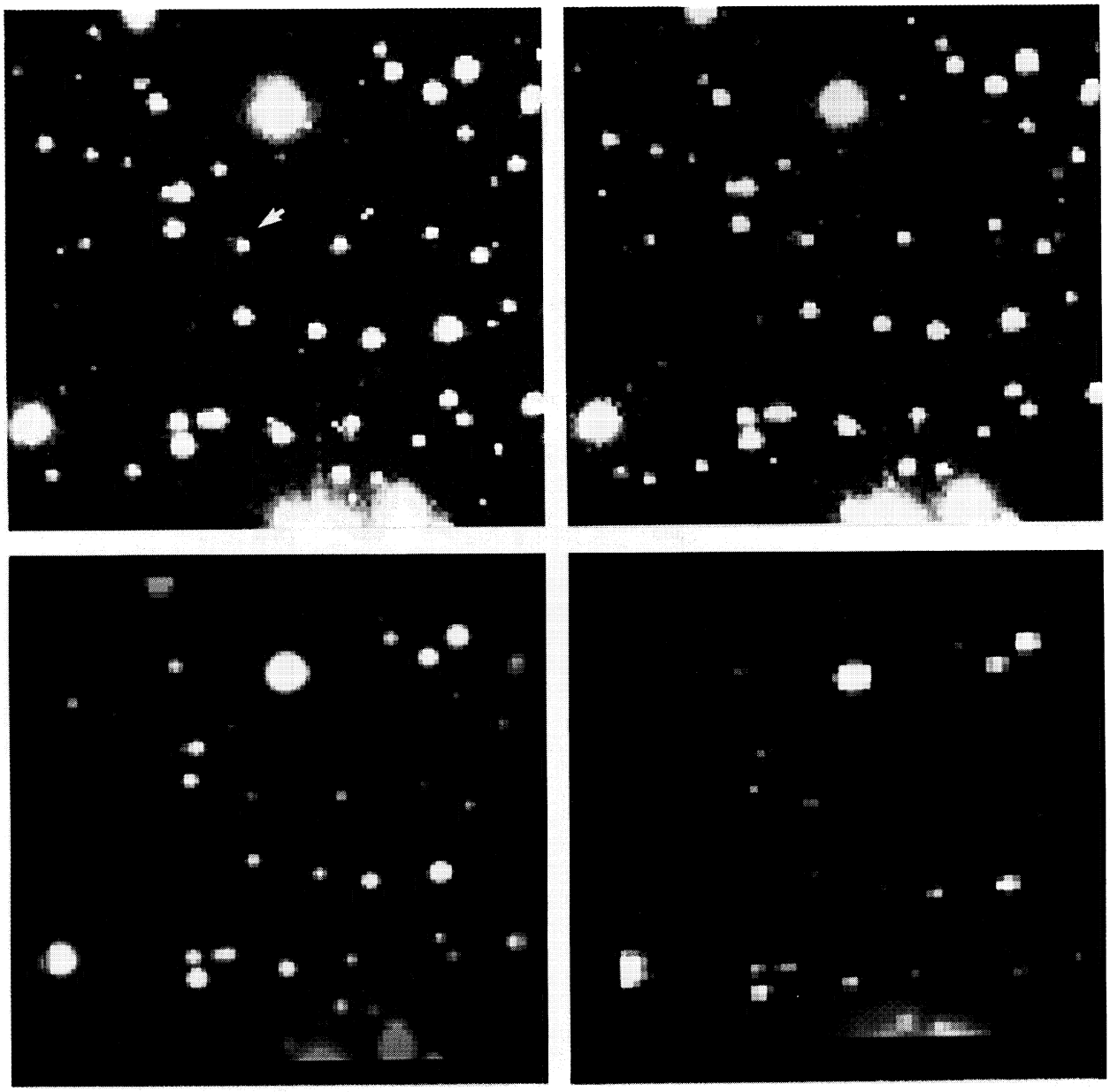

FIG. 1. The field of GT 0116 + 622, imaged at visible and near-IR wavelengths with CCD and InSb array detectors. The IR data, originally of scale 1.3″ pixel^{-1}, have been remapped with flux conservation to match the 0.86″ pixel^{-1} scale of the CCD data. Each field is $\sim 80 \times 80''$, with north up and east to the left. *Upper left*: a 1200 s CCD exposure in the Johnson *R*-band; the arrow indicates the proposed counterpart to the radio source, a stellar object, and $\sim 3''$ of fuzz extended to the east. *Upper right*: a 1200 s CCD image in the Johnson *I*-band. Note that the fuzz becomes more prominent, indicating large $(R - I)$. *Lower left*: A superposition of the *R* and *I* images with a co-added 4800 s *J* image. The CCD data point-spread functions have been degraded to match that of the *J* image. The three bands are color-coded blue, green, and red, respectively, to mimic their increasing wavelengths; the colors have been crudely balanced so that an average field object is neutral. It is clear that the fuzz is significantly redder than the point source, and asymmetrically placed. The CCD images include slightly more field than the IR images; this lack of overlapping data at the boundaries explains the anomalously blue colors of stars there. The diffuse arc near the south border is scattered light from two bright stars. *Lower right*: A superposition of the summed *J*, *H*, and *K* data, again color-coded blue, green, and red, respectively, to mimic the wavelength relationship of the bands. Note that the fuzz now overwhelms the point source, and is far redder than any other object in the field.

Margon *et al.* (see page 925)